

Three 3D Metal-Organic Frameworks Constructed from Keggin Polyanions and Multi-nuclear Ag^I Clusters: Assembly, Structures and Properties

Xiu-Li Wang, Na Li, Ai-Xiang Tian, Jun Ying, Guo-Cheng Liu, Hong-Yan Lin, and Dan Zhao

Department of Chemistry, Bohai University, Liaoning Province Silicon Materials Engineering Technology Research Center, Jinzhou 121013, P. R. China

Reprint requests to Dr. Xiu-Li Wang. E-mail: wangxiuli@bhu.edu.cn

Z. Naturforsch. **2013**, 68b, 778 – 788 / DOI: 10.5560/ZNB.2013-3007

Received January 10, 2013

Three Keggin-based metal-organic frameworks (MOFs) containing multi-nuclear silver subunits, [Ag₇(ptz)₅(H₂O)₂][H₂SiMo₁₂O₄₀] (**1**), [Ag₈(ptz)₅(H₂O)₂][AsW₁₂O₄₀] (**2**) and [Ag₇(ptz)₅(H₂O)][HAsMo₁₂O₄₀] (**3**) (ptzH = 5-(4-pyridyl)-tetrazole), have been synthesized under hydrothermal conditions by changing the inorganic polyanions. The new compounds have been characterized by elemental analyses, TG analyses, IR spectroscopy, and single-crystal X-ray diffraction. In compound **1**, the multi-nuclear Ag₅(ptz)₅ subunits are interconnected to form chains, which are further linked by Ag^I cations to construct a 3D MOF with large channels. Pairs of SiMo₁₂O₄₀^{4−} polyanions reside in the channels as penta-dentate inorganic ligands. In **2**, six Ag^I cations link five ptz[−] anions to construct a hexa-nuclear subunit [Ag₆(ptz)₅]⁺, which is interconnected to form chains. These chains are further linked by Ag^I cations to construct a 3D MOF, where AsW₁₂O₄₀^{3−} polyanions reside as hexa-dentate ligands. Compound **3** exhibits a 3D MOF based on Ag₅(ptz)₅ subunits, in which the hexa-dentate AsMo₁₂O₄₀^{3−} polyanions are incorporated. The rigid tetrazole-based ligand ptz[−] plays an important role in the formation of the multi-nuclear subunits of the title compounds. The electrochemical properties of compound **1** and the photocatalytic properties of compounds **1** and **3** have been investigated.

Key words: Keggin Polyoxometalate, Tetrazole-based Ligand, Metal-Organic Framework, Photocatalytic Properties, Electrochemical Properties

Introduction

Polyoxometalates (POMs), as a kind of discrete metal oxide clusters with abundant structural diversity, have received great attention in recent years [1–3]. Among the many types of POMs, the Keggin-type polyanions, possessing diverse electronic, magnetic, photochemical, and catalytic properties, have been regarded as important inorganic building blocks or templates to construct novel metal-organic frameworks (MOFs), and many high-dimensional frameworks have been obtained [4, 5]. To our knowledge, however, POM-supported MOFs containing multi-nuclear metal clusters are still relatively scarce [6, 7]. Thus, there is a challenge to reasonably design and construct novel POM-based MOFs with multi-nuclear metal clusters and Keggin polyanions.

The appropriate selection of transition metal ions and organic ligands may induce the formation of multi-nuclear structures. Ag^I as a *d*¹⁰ transition metal cation exhibits various coordination modes and can form multi-nuclear metal clusters with ease [8–11]. Therefore, for this work, we have selected Ag^I salts as reactants aiming at the construction of multi-nuclear Ag^I clusters. On the other hand, the structure of organic ligands is essential for the construction of multi-nuclear clusters. Ligands with many adjacent coordination sites usually tend to favor multi-nuclear clusters, because the concentration of coordination sites conduces to collect metal ions. In our previous work, we have employed flexible bis(tetrazole) ligands as the organic moieties and obtained a series of novel complexes based on Keggin polyanions and Ag^I-bis(tetrazole) multi-nuclear subunits [12–15] in which

the ligands just meet the character required for forming multi-nuclear clusters. We also introduced 1*H*-1,2,3-benzotriazole into the POM system and obtained two 2D POM-based networks containing multi-nuclear clusters [16]. In order to continuously explore the role of rigid multi-dentate *N*-donor ligands in the POM-multi-nuclear cluster system, for this work, we have selected 5-(4-pyridyl)-tetrazole (ptzH) as a rigid organic moiety with four adjacent N donors (Scheme S1 in the Supporting Information available online; see note at the end of the paper for availability) to enhance the capacity of collecting metal ions, aiming at investigating whether multi-nuclear subunits can be obtained in POM-based complexes. The pyridyl group of ptzH may play a role in dimensional extension. To our knowledge, only Peng's group reported several examples combining Ag-ptz multi-nuclear subunits and POMs [17]. Yan's group reported a series of POM-based complexes containing Ag-ptz metal-organic subunits, but with the N atom of a pyridyl group in different position [18].

Herein, three Keggin-type POMs, *i. e.* $[\text{H}_4\text{SiMo}_{12}\text{O}_{40}] \cdot 26\text{H}_2\text{O}$, $[\text{H}_3\text{AsW}_{12}\text{O}_{40}] \cdot 26\text{H}_2\text{O}$ and $[\text{H}_3\text{AsMo}_{12}\text{O}_{40}] \cdot 26\text{H}_2\text{O}$, were used as starting materials for the inorganic ligands, and ptzH (ptzH = 5-(4-pyridyl)-tetrazole) was used as the organic ligand precursor. They were reacted with Ag^{I} cations under hydrothermal conditions. As a result, three 3D Keggin-based MOFs, $[\text{Ag}_7(\text{ptz})_5(\text{H}_2\text{O})_2][\text{H}_2\text{SiMo}_{12}\text{O}_{40}]$ (**1**),

$[\text{Ag}_8(\text{ptz})_5(\text{H}_2\text{O})_2][\text{AsW}_{12}\text{O}_{40}]$ (**2**) and $[\text{Ag}_7(\text{ptz})_5(\text{H}_2\text{O})][\text{HAsMo}_{12}\text{O}_{40}]$ (**3**) have been obtained. The photocatalytic and electrochemical properties of compounds **1** and **3** have been investigated.

Results and Discussion

Crystal structure of compound **1**

The crystal structure analysis reveals that compound **1** consists of seven Ag^{I} cations, five ptz^- anions, two coordinated water molecules, and one $[\text{H}_2\text{SiMo}_{12}\text{O}_{40}]^{2-}$ (abbreviated to SiMo_{12}) anion. The valence sum calculations [19] show that all the Mo atoms are in the +VI oxidation state, all the Ag atoms are in the +I oxidation state, and each ptzH ligand precursor has lost a proton to act as ptz^- anion. Similar to the cases of $[\text{Ag}_7(\text{ptz})_5(\text{H}_2\text{SiW}_{12}\text{O}_{40})(\text{H}_2\text{O})]$ [17] and also $[\text{Cu}(\text{bimb})_2(\text{HPW}_{12}\text{O}_{40}) \cdot 3\text{H}_2\text{O}]$ [20], two H atoms are added to the $[\text{SiMo}_{12}\text{O}_{40}]^{4-}$ anion in order to balance the charges. Protonation of POMs is a common phenomenon in POM-based compounds (see also the Experimental Section).

In compound **1**, the SiMo_{12} anion acts as a penta-dentate inorganic ligand to link one Ag4, one Ag7 and three Ag6 cations, as shown in Fig. 1a. Seven crystallographically independent Ag^{I} cations adopt four kinds of coordination geometries (Fig. 1b and Table 1): (i) The Ag1 cation is two-coordinated by

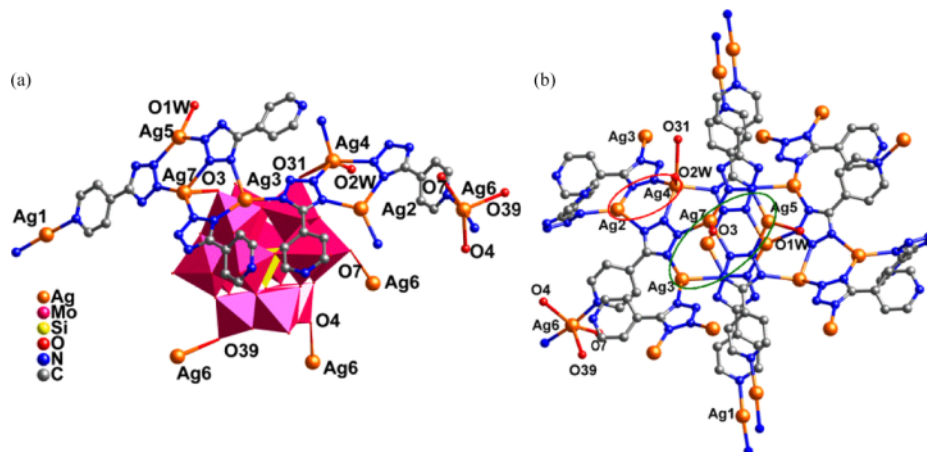


Fig. 1 (color online). (a) Ball-and-stick and polyhedral representation of the structural unit of compound **1** and the coordination environment of the Ag^{I} cations (H atoms were omitted for clarity); (b) the multi-nuclear subunit in **1** containing $[\text{Ag}_3(\text{ptz})_3]$ and $[\text{Ag}_2(\text{ptz})_2]$ clusters, showing the coordination modes of Ag^{I} cations and ptz^- anions in compound **1** (the crystal water and hydrogen atoms are omitted for clarity; red cycle: a bi-nuclear subunit $[\text{Ag}_2(\text{ptz})_2]$, green cycle: a tri-nuclear subunit $[\text{Ag}_3(\text{ptz})_3]$).

two N atoms (N5 and N9) from the pyridyl groups of two ptz^- anions in a linear mode. The bond lengths and angles are 2.132(5) and 2.126(5) Å for Ag–N and 174.4(2)° for N–Ag–N. (ii) The Ag2, Ag3 and Ag5 cations all adopt a similar three-coordination mode in a T-type geometry. The Ag2 and Ag3 cations are coordinated by three N atoms (N14, N18, N23 for Ag2 and N4, N22, N20 for Ag3) from the tetrazole groups of three different ptz^- anions, with Ag2–N distances of 2.234(5)–2.305(5) Å and Ag3–N distances of 2.190(5)–2.444(5) Å, N–Ag2–N angles of 113.10(17)–126.09(18)° and N–Ag3–N angles of 104.47(17)–148.84(19)°. The Ag5 cation is coordinated by two N atoms (N1 and N21) from the tetrazole groups of two ptz^- anions and by one water molecule. The bond lengths and angles around Ag5 are 2.187(6) and 2.234(5) Å for Ag–N, 2.393(12) Å for Ag–O, 124.3(2)° for N–Ag–N, and 103.7(3)–129.3(3)° for N–Ag–O. (iii) Both Ag4 and Ag6 cations are five-coordinated in trigonal bipyramidal geometries. The Ag4 cation is coordinated by three N atoms (N7, N12 and N16) from the tetrazole groups of three ptz^- anions, one terminal oxygen atom (O31) from one SiMo_{12} anion and one water molecule. The distances and angles around the Ag4 cation are 2.297(5)–2.390(5) Å for Ag–N, 2.409(10)–2.804(10) Å for Ag–O, 105.31(18)–111.22(18)° for N–Ag–N and 78.8(3)–138.5(3)° for N–Ag–O. The Ag6 cation is

coordinated by two N atoms (N10 and N25) from the pyridyl groups of two ptz^- anions and three O atoms (O4, O7 and O39) from one SiMo_{12} anion, with Ag–N distances of 2.136(5) and 2.161(5) Å, Ag–O distances of 2.586(4)–2.682(4) Å, an N–Ag–N angle of 169.9(2)°, and N–Ag–O angles of 85.42(17)–98.16(18)°. (iv) The Ag7 cation is coordinated in a “seesaw” geometry by three N atoms from the tetrazole groups of three ptz^- anions and one oxygen atom from one SiMo_{12} anion with Ag–N distances of 2.210(6)–2.377(5) Å and an Ag–O distance of 2.552(4) Å. These distances are comparable to those in other Ag^{I} compounds [21].

In compound **1**, the ptz^- anions exhibit four types of coordination modes (Fig. 2): a-type (green), b-type (purple), c-type (red) and d-type (blue) modes. The a-type ptz^- endows two N donors of the tetrazole group (N10 and N14) to fuse two Ag cations, while b-type ptz^- provides three N donors of the tetrazole group to integrate three Ag cations. The c-type ptz^- provides three N donors from the tetrazole and pyridyl groups to integrate three Ag cations. The d-type ptz^- is a highly efficient ligand, which offers all its N donors not only from the tetrazole group but also from the pyridyl group to coordinate with five Ag cations. The N donor atoms of the tetrazole group are in charge of collecting Ag cations, while the N atom in the pyridyl group plays the linkage role. The structural character and strong coordination ability of the ptz^- anion promote the for-

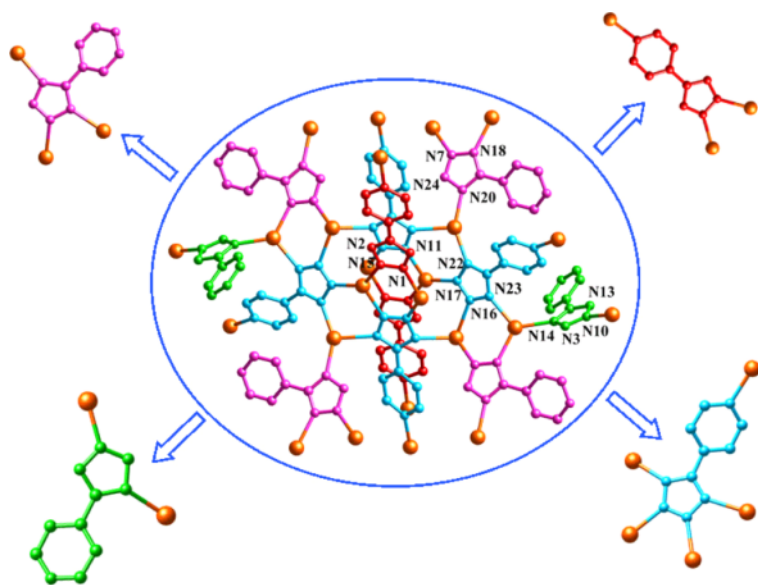


Fig. 2 (color online). Four types of coordination modes of ptz^- anions in the multi-nuclear subunit of **1**: a-type (green), b-type (purple) c-type (red) and d-type (blue).

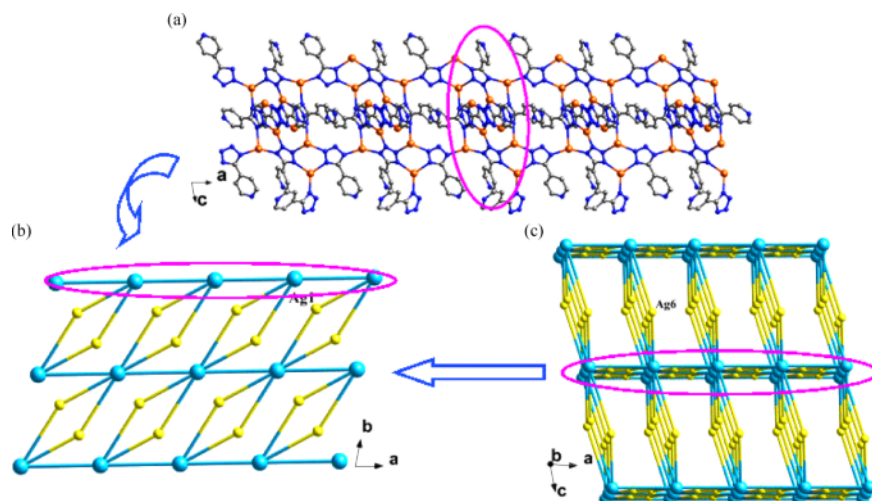


Fig. 3 (color online). (a) The multi-nuclear chain in **1**; (b) the 2D grid-like network formed by a multi-nuclear chain and Ag1 cations (yellow); (c) the 3D MOF extended by Ag6 cations.

mation of multi-nuclear clusters. As shown in Fig. 1b and Fig. S1 (Supplementary Information, available online), Ag3, Ag5 and Ag7 are linked by three ptz[−] anions to form a tri-nuclear subunit [Ag₃(ptz)₃], while Ag2 and Ag4 are linked by two ptz[−] anions to form a bi-nuclear subunit [Ag₂(ptz)₂]. The [Ag₃(ptz)₃] and [Ag₂(ptz)₂] clusters are connected through sharing the same ptz[−] anions to generate a special multi-nuclear subunit [Ag₅(ptz)₅]. There are also many face-to-face aryl packing interactions between pyridyl groups of the ptz[−] anions, which can be viewed as an important factor for stabilizing the multi-nuclear structure (Fig. S2). These π – π stacking distances vary from 3.6 to 3.9 Å.

The multi-nuclear subunits [Ag₅(ptz)₅] are connected through sharing the same ptz[−] anions, leading to the formation of a multi-nuclear chain (Fig. 3a). These chains are connected *via* Ag1 cations to form 2D grid-like networks (Fig. 3b, Fig. S3), which are further extended into a 3D MOF with large channels by an Ag6-ptz linkage (Fig. 3c). The SiMo₁₂ anion, acting as a five-connected inorganic ligand, offers five terminal oxygen atoms to coordinate with the Ag^I cations of the 3D MOF and resides in the “distorted” rectangular channels (Fig. 4).

It is noted that the channels of the 3D MOF are double-occupied by Keggin SiMo₁₂ anions. To date, only few examples of double Keggin-supported/templated MOFs have been reported. For example, Peng’s group used double Keggin anions as templates to construct a 3D MOF [17]. Wang’s

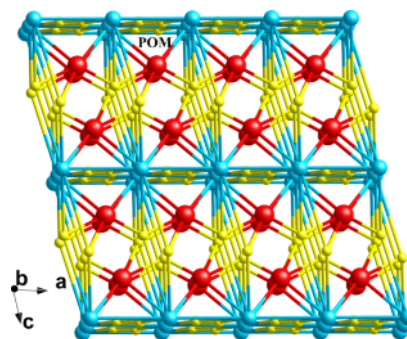


Fig. 4 (color online). The SiMo₁₂ anions (red) acting as penta-dentate inorganic ligands incorporated in the “distorted” rectangular channels of 3D MOF.

group reported a double-Keggin POM-templated, molybdenum-oxide-based inorganic-organic hybrid compound [22]. Our group also reported two metal-organic complexes based on double Keggin-type polyoxometalate templates [23]. The formation of the multi-nuclear framework of **1** has thus proven that the synthetic strategy for preparing POM-supported MOFs containing multi-nuclear clusters is rational.

Crystal structures of compounds **2** and **3**

In order to further explore the influence of different Keggin polyanions on the POM multi-nuclear cluster system, we selected different Keggin polyanions as inorganic ligands, aiming at obtaining new POM-supported MOFs containing multi-

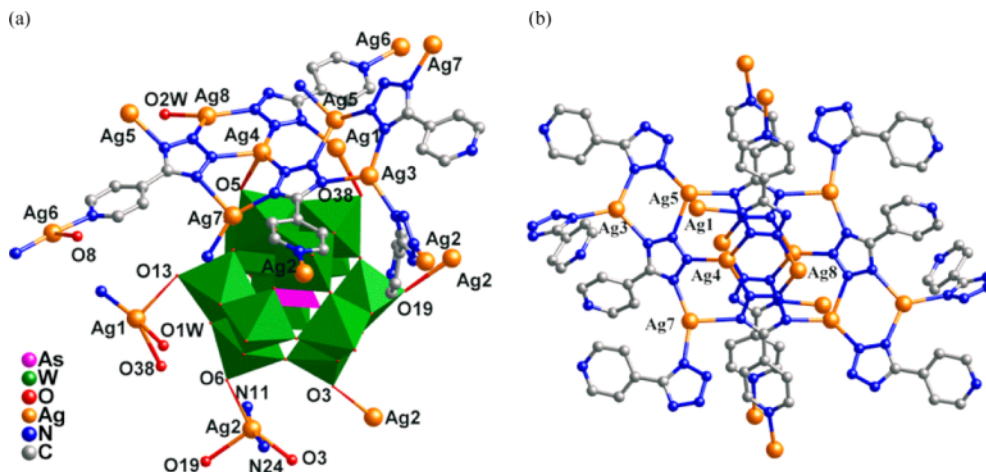


Fig. 5 (color online). (a) Ball-and-stick and polyhedral representation of the structural unit of compound **2** and the coordination environment of the Ag^{I} cations (H atoms were omitted for clarity); (b) the multi-nuclear subunit $[\text{Ag}_6(\text{ptz})_5]^+$ in **2**.

nuclear clusters. When the SiMo_{12} anion was replaced by $[\text{AsW}_{12}\text{O}_{40}]^{3-}$ (AsW_{12}) and $[\text{AsMo}_{12}\text{O}_{40}]^{3-}$ (AsMo_{12}) anions, respectively, compounds **2** and **3** were obtained. The valence sum calculations [19] show that all the W atoms in **2** and all the Mo atoms in **3** are in the +VI oxidation state, and all the Ag atoms are in the +I oxidation state. Similar to compound **1**, all ptzH ligands in **2** and **3** have lost a proton and carry a -1 charge. In **2** the POM anion exists as $[\text{AsW}_{12}\text{O}_{40}]^{3-}$ while in **3** it must be the mono-protonated anion $[\text{HAsMo}_{12}\text{O}_{40}]^{2-}$.

Crystal structure analysis reveals that compound **2** contains eight crystallographically independent Ag^{I} cations, five ptz^- anions, two coordinated water molecules, and one AsW_{12} anion, as shown in Fig. 5a. The Ag^{I} cations show three types of coordination modes, and the ptz^- anions exhibit four types of coordination modes (Table 1). In compound **2**, six Ag^{I} cations are connected together through five ptz^- anions to generate a hexa-nuclear subunit $[\text{Ag}_6(\text{ptz})_5]^+$ (Fig. 5b). The hexa-nuclear subunits are connected to form chains, which are further linked by Ag^{I} cations to construct a 3D MOF, where AsW_{12} polyanions reside as hexa-dentate ligands (Table 1).

Compound **3** consists of seven Ag^{I} cations, five ptz^- anions, one coordinated water molecule, and one AsMo_{12} anion (Fig. S4). Although crystals of compound **3** possesses the same space group and dimensions and the same 2D Ag-ptz layer as those of the reported compound $[\text{Ag}_7(\text{ptz})_5(\text{H}_2\text{SiW}_{12}\text{O}_{40})$

$(\text{H}_2\text{O})]$ [17], the Keggin anions in **3** act as hexa-dentate inorganic ligands, while the Keggin anions in $[\text{Ag}_7(\text{ptz})_5(\text{H}_2\text{SiW}_{12}\text{O}_{40})(\text{H}_2\text{O})]$ act as tetra-dentate ligands. That is to say, compound **3** exhibits a 3D framework with hexa-coordinate anions residing in the channels (Table 1).

IR spectra

The IR spectra of compounds **1–3** are shown in Fig. S5. For compound **1**, the IR spectrum exhibits the characteristic bands of the Keggin structure at 970, 908, 777, and 1015 cm^{-1} , which can be attributed to $\nu(\text{Mo}-\text{O}_t)$, $\nu(\text{Mo}-\text{O}_b-\text{Mo})$, $\nu(\text{Mo}-\text{O}_c-\text{Mo})$, and $\nu(\text{Si}-\text{O})$, respectively. The characteristic bands at 970, 908, 786, and 1040 cm^{-1} of compound **2** are attributed to $\nu(\text{W}-\text{O}_t)$, $\nu(\text{W}-\text{O}_b-\text{W})$, $\nu(\text{W}-\text{O}_c-\text{W})$, and $\nu(\text{As}-\text{O})$, while the bands at 962, 886, 771, and 962 cm^{-1} in compound **3** are attributed to $\nu(\text{Mo}-\text{O}_t)$, $\nu(\text{Mo}-\text{O}_b-\text{Mo})$, $\nu(\text{Mo}-\text{O}_c-\text{Mo})$, and $\nu(\text{As}-\text{O})$, respectively [24]. The bands at $1456\text{--}1698\text{ cm}^{-1}$ are characteristic of the ptz^- anions for **1**, at $1460\text{--}1698\text{ cm}^{-1}$ for **2** and at $1450\text{--}1695\text{ cm}^{-1}$ for **3** [25].

TG analyses

The thermogravimetric (TG) analyses of **1–3** were carried out in flowing N_2 with a heating rate of $10^\circ\text{C min}^{-1}$ in the temperature range of $20\text{--}800^\circ\text{C}$, as shown in Fig. S6. The title compounds **1–3** show


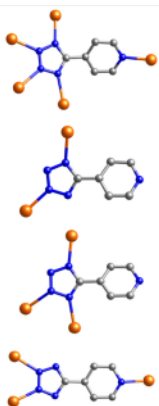
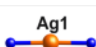


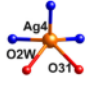
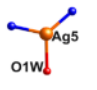
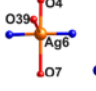
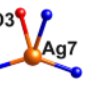
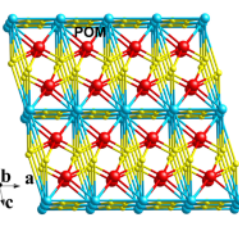
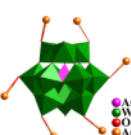
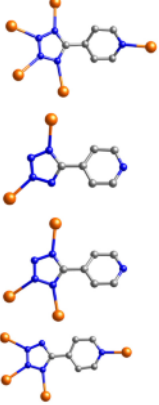
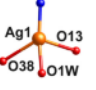


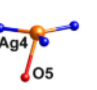
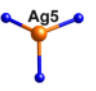
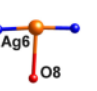


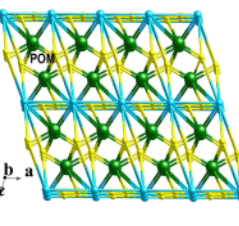
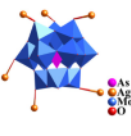
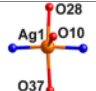

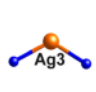
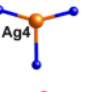
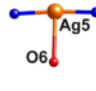

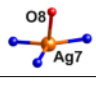
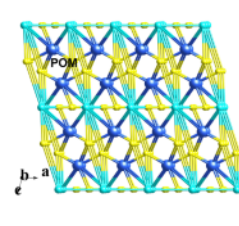
	Coordination modes of POMs	Coordination modes of ptz [−] anions	Coordination modes of silver cations	3D POM-based frameworks
1			      	
2			       	
3		Same as compound 1	      	

Table 1. The coordination modes of POMs, ptz[−] anions and Ag^I cations, as well as the frameworks in the crystal structures of **1–3**.

two distinct weight loss steps. The first weight loss steps occur before 250 °C, which correspond to the loss of coordinated water molecules, 1.1% (calcd. 1.1%) in **1**, 0.8% (calcd. 0.8%) in **2** and 1.6% (calcd.

0.5%) in **3**. The second weight loss steps at 250–680 °C correspond to the loss of organic ligands, 21.8% (calcd. 21.9%) in **1**, 16.1% (calcd. 16.1%) in **2** and 21.6% (calcd. 21.7%) in **3**.

Photoluminescence spectra

The fluorescence properties of compounds **1–3** and of the free ptzH molecule have been investigated at room temperature. The ptzH molecule shows a strong emission at 350 nm upon excitation at 330 nm, which may be assigned to the intraligand charge transfer (Fig. S7, inset). As shown in Fig. S7, for compound **1**, the maximum emission peak is observed at 438 nm upon excitation at 350 nm. When excited by 360 nm light, compound **2** displays a strong emission band at 468 nm, while the emission band of compound **3** is at 457 nm upon excitation at 350 nm. Compared with free ptzH, the significant red-shifts for compounds **1–3** may be due to the deprotonation of ptzH and the coordination of the ptz[−] anions to the Ag^I cations, which decreases the HOMO-LUMO separation of the title compounds [18].

Electrochemical properties

The electrochemical properties of compound **1** as a bulk-modified carbon paste electrode (**1-CPE**) was investigated in 0.5 M H₂SO₄ aqueous solution at different scan rates. As shown in Fig. 6a, in the potential range of +700 to −150 mV, there exist three reversible redox peaks I–I', II–II' and III–III', with the mean peak potentials $E_{1/2} = (E_{pa} + E_{pc})/2$ of +299, +189, and −19 mV (scan rate: 80 mV s^{−1}), corresponding to three consecutive two-electron processes of the SiMo₁₂ anion [15]. The peak potentials change gradually following the scan rates from 20 to 400 mV s^{−1}: the cathodic peak potentials shift towards the negative direction and the corresponding anodic peak potentials to the positive direction with increasing scan rates. When the scan rates are lower than 400 mV s^{−1}, the peak currents are proportional to the scan rates, which indicate that the redox process of **1-CPE** is surface-confined (Fig. S8). It's well known that POMs are excellent electrocatalytic materials [23, 26, 27]. In this work, we found that **1-CPE** has good electrocatalytic activity toward the reduction of nitrite, as shown in Fig. 6b. With the addition of nitrite, all the reduction peak currents increase, and the corresponding oxidation peak currents decrease dramatically, which indicates that all the reduced species of the SiMo₁₂ anions in **1** possess electrocatalytic activity toward the reduction of nitrite. Hence compound **1** may be used as a potential electrocatalyst.

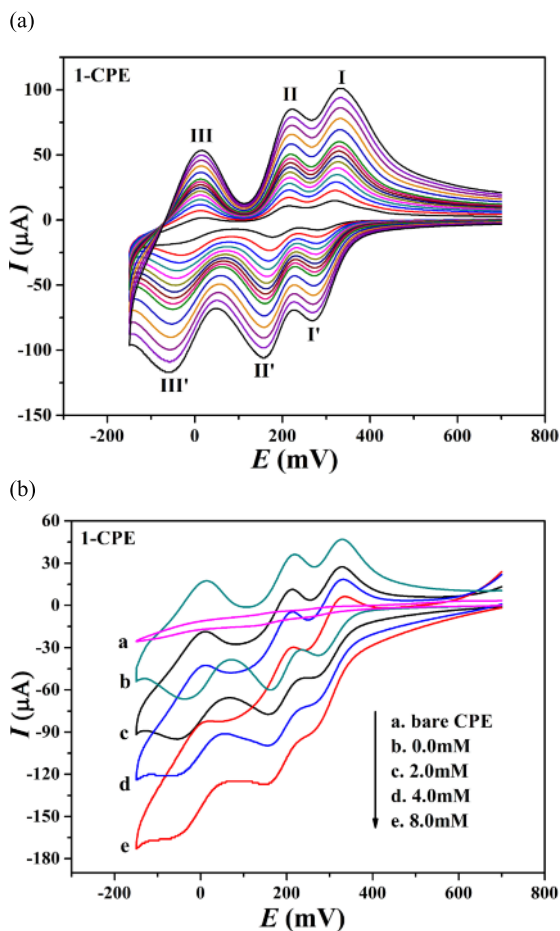


Fig. 6 (color online). (a) The cyclic voltammograms of **1-CPE** in 0.5 M H₂SO₄ aqueous solution at different scan rates (from inner to outer: 20, 40, 60, 80, 100, 120, 140, 160, 180, 200, 250, 300, 350, and 400 mV s^{−1}); (b) cyclic voltammograms of a bare CPE in 0.5 mM KNO₂ + 0.5 M H₂SO₄ aqueous solution (a) and of **1-CPE** in 0.5 M H₂SO₄ aqueous solution containing 0 (b); 2 (c); 4 (d); 8 (e) mM KNO₂. Scan rate: 120 mV s^{−1}.

Photocatalytic activities

With the rapid development of POM-based inorganic-organic hybrids, more and more attention has been concentrated on their specific properties for potential applications. POMs, as a kind of green catalysts, have been widely used in the degradation of organic dyes [28]. Therefore, the photocatalytic degradation of the organic dye pollutant methylene blue (MB) under UV light irradiation was investigated by using compound **1** or **3** as photocatalyst. A typical process is as follows: Compound **1** or **3** (150 mg) was

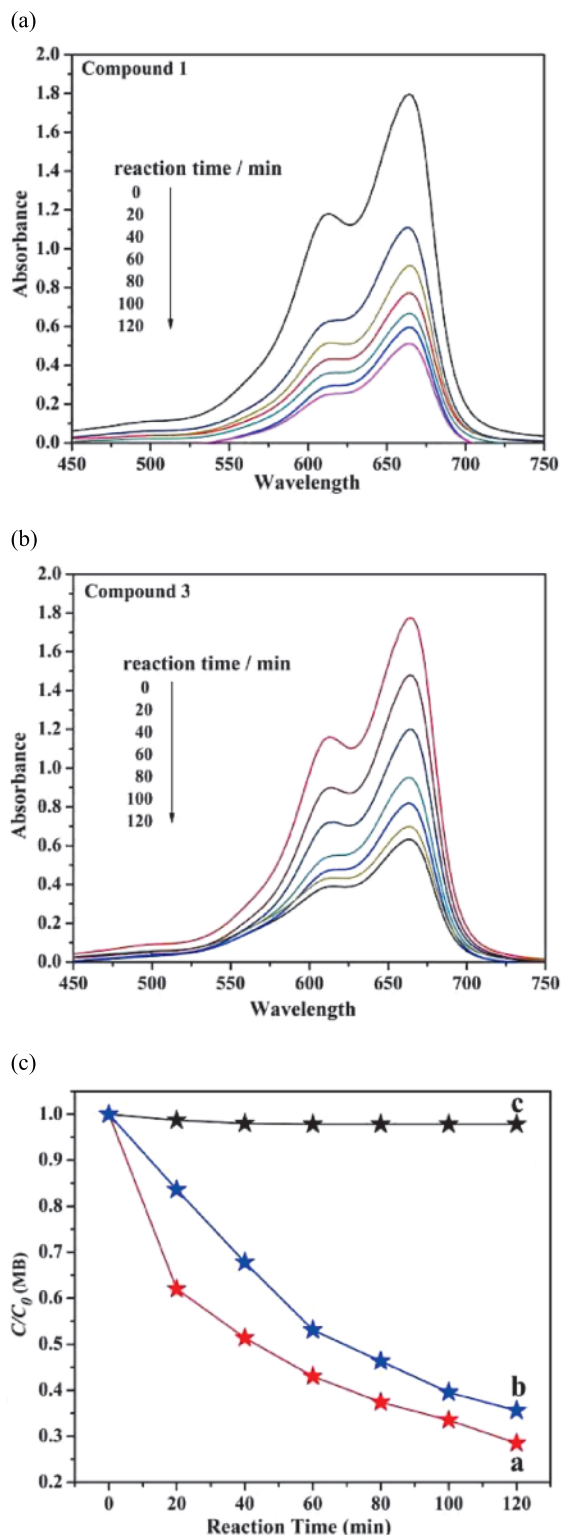


Fig. 7 (color online). (a) Absorption spectra of the methylene blue (MB) solution during the decomposition reaction under UV light irradiation with the use of compound **1**; (b) absorption spectra of the MB solution with the use of compound **3**; (c) C/C_0 vs. t curves of MB photocatalytic degradation (a: compound **1**, b: compound **3**, c: MB only).

dispersed in 90 mL MB solution (10.0 mg L^{-1}) and magnetically stirred for about 30 min to ensure the equilibrium. Then the mixed solution was irradiated with a high-pressure mercury vapor lamp for 120 min, while kept stirring. 3.0 mL samples were taken out every 20 min and scanned in a UV spectrophotometer. The results have shown that the absorption peaks of MB decrease over time (Fig. 7). The photocatalytic properties of the MB solution without compounds **1** or **3** were also investigated under the same conditions. The results show that MB degradation can be up to 71 % for **1** and 64 % for **3** after 120 min under UV light irradiation, while the absorption peaks of MB without any catalyst show no obvious change, indicating that compounds **1** or **3** as photocatalysts provide a new way for the removal of aqueous organic dye pollutants.

Conclusions

In this work, we have successfully constructed three POM-based inorganic-organic hybrids containing multi-nuclear Ag^{I} clusters. Compound **1** shows a 3D MOF with large channels with five-connected SiMo_{12} anions residing in them. Compound **1** owns $[\text{Ag}_5(\text{ptz})_5]$ subunits, while **2** contains $[\text{Ag}_6(\text{ptz})_5]^+$ and **3** contains $[\text{Ag}_5(\text{ptz})_5]$ subunits in the 3D MOF. In these compounds, both the polyanions and the ptz^- ligands exhibit a variety of coordination modes. The successful syntheses of these three POMs-based compounds indicate that using the rigid tetrazole-based ligand and different Keggin polyanions is an effective strategy for obtaining high-dimensional structures containing multi-nuclear metal clusters. Compounds **1** and **3** may be used as electro- and photocatalysts. Further studies on tuning the properties by constructing new POM-based multi-nuclear structures are underway.

Experimental Section

Materials and measurements

All reagents and solvents for syntheses were purchased and used without further purification. Elemental analyses

were carried out with a Perkin-Elmer 240C elemental analyzer, and the FT-IR spectra were recorded on a Magna FT-IR 560 spectrometer (KBr pellets). The thermal gravimetric analyses (TGA) were carried out in N₂ on a Pyris-Diamond thermal analyzer with a rate of 10 °C min⁻¹. Electrochemical measurements and data collection were performed with a CHI 440 electrochemical workstation connected to a Digital-586 personal computer. A conventional three-electrode system was used with a saturated calomel electrode (SCE) as reference electrode and a Pt wire as counter electrode. Chemically bulk-modified carbon paste electrodes (CPEs) were used as the working electrodes. UV/Vis absorption spectra were obtained using a SP-1900 UV/Vis spectrophotometer.

Synthesis of [Ag₇(ptz)₅(H₂O)₂][H₂SiMo₁₂O₄₀] (**1**)

A mixture of H₄SiMo₁₂O₄₀·26H₂O (0.16 g, 0.07 mmol), AgNO₃ (0.13 g, 0.8 mmol), and ptzH (0.04 g, 0.28 mmol) was dispersed in 10 mL of distilled water at room temperature. The pH value of the mixture was adjusted to about 2.5 with 1.0 mol L⁻¹ HNO₃, and the suspension was sealed into a 20 mL Teflon-lined autoclave and kept under autogenous pressure at 160 °C for 4 d. After slow cooling to room temperature, yellow block-shaped crystals of **1** were obtained, filtered and washed with distilled water (30% yield based on Mo). – Elemental analysis (%) for C₃₀H₂₆Ag₇N₂₅O₄₂SiMo₁₂: calcd. C 10.77, H 0.78, N 10.47; found C 10.68, H 0.62, N 10.58. – IR (solid KBr pellet, cm⁻¹), ν = 1685(m), 1633(m), 1508(m), 1456(m), 1018(m), 970(m), 908(s), 848(m), 777(s), 669(m).

Synthesis of [Ag₈(ptz)₅(H₂O)₂][AsW₁₂O₄₀] (**2**)

Compound **2** was prepared similarly, except that H₃AsW₁₂O₄₀·26H₂O (0.33 g, 0.11 mmol) was used instead of H₄SiMo₁₂O₄₀·26H₂O. Red block-shaped crystals of **2** were obtained in 31% yield (based on W). – Elemental analysis (%) for C₃₀H₂₄Ag₈N₂₅O₄₂AsW₁₂: calcd. C 7.91, H 0.53, N 7.79; found C 7.84, H 0.50, N 7.69. – IR (KBr pellet, cm⁻¹), ν = 1698(w), 1633(w), 1516(m), 1460(w), 970(m), 908(s), 852(w), 786(s), 669(w).

Synthesis of [Ag₇(ptz)₅(H₂O)][HAsMo₁₂O₄₀] (**3**)

Compound **3** was prepared similarly, except that H₃AsMo₁₂O₄₀·26H₂O (0.21 g, 0.11 mmol) was used instead of H₃AsW₁₂O₄₀·26H₂O. Red block-shaped crystals of **3** were obtained in 34% yield (based on Mo). – Elemental analysis (%) for C₃₀H₂₃Ag₇N₂₅O₄₁AsMo₁₂: calcd. C 10.68, H 0.68, N 10.38; found C 10.65, H 0.53, N 10.38. – IR (KBr pellet, cm⁻¹), ν = 1695(m), 1634(s), 1541(m), 1503(w), 962(s), 886(s), 837(m), 771(s), 690(w), 581(m).

X-Ray crystallography

Intensity data for compounds **1–3** were collected on a Bruker Smart 1000 CCD diffractometer with MoK α radiation (λ = 0.71073 Å) in ω - and θ -scan mode at 293 K. All the structures were solved by Direct Methods and refined on F^2 by full-matrix least-squares methods using the SHELXTL package [29]. All non-hydrogen atoms were refined anisotropically. The H atoms attached to carbon atoms were generated geometrically while the H atoms attached to water molecules were not located. Likewise, the H atoms

Table 2. Crystal data and numbers pertinent to data collection and structure refinement for compounds **1–3**.

	1	2	3
Formula	C ₃₀ H ₂₆ Ag ₇ N ₂₅ O ₄₂ SiMo ₁₂	C ₃₀ H ₂₄ Ag ₈ N ₂₅ O ₄₂ AsW ₁₂	C ₃₀ H ₂₃ Ag ₇ N ₂₅ O ₄₁ AsMo ₁₂
M_r	3343.22	4550.82	3371.02
Crystal system	triclinic	triclinic	triclinic
Space group	$P\bar{1}$	$P\bar{1}$	$P\bar{1}$
a , Å	12.0117(11)	12.0216(9)	12.042(3)
b , Å	13.9360(12)	13.9379(11)	13.967(3)
c , Å	22.602(2)	22.7658(17)	22.754(5)
α , deg	77.088(2)	95.8250(10)	95.802(4)
β , deg	74.6570(10)	104.7220(10)	105.211(4)
γ , deg	75.5240(10)	104.0360(10)	104.118(4)
V , Å ³	3482.2(6)	3524.7(5)	3525.2(13)
Z	2	2	2
D_{calcd} , Mg cm ⁻³	3.19	4.29	3.18
μ (MoK α), mm ⁻¹	4.1	22.2	4.5
$F(000)$, e	3128	4024	3144
R_1 / wR_2 [$I > 2 \sigma(I)$]	0.0308 / 0.0772	0.0603 / 0.1470	0.0803 / 0.2115
R_1 / wR_2 (all data)	0.0333 / 0.0784	0.1011 / 0.1680	0.1124 / 0.2444
GOF on F^2	1.067	1.037	0.939
Largest diff. peak / hole, e Å ⁻³	4.58 / -1.92	3.54 / -4.21	4.85 / -2.09

of the protonated POM anions $[\text{H}_2\text{SiMo}_{12}\text{O}_{40}]^{2-}$ in **1** and $[\text{HAsMo}_{12}\text{O}_{40}]^{2-}$ in **3** were not located. In these cases, the H atoms are commonly considered to be associated with the POM anions [17, 20, 30–32]. A summary of crystal data and structure refinements for the title compounds are given in Table 2. Selected bond lengths (Å) and angles (deg) of the three compounds are listed in the Supporting Information Table S1.

CCDC 907616, 907618 and 907617 (**1–3**) contain the supplementary crystallographic data for this paper. These data can be obtained free of charge from The Cambridge Crystallographic Data Centre via www.ccdc.cam.ac.uk/data_request/cif.

Preparation of bulk-modified CPE of compound **1**

The bulk-modified CPE of **1** (1-CPE) was fabricated as follows [33]: 100 mg of graphite powder and 10 mg of **1** were mixed and ground together by agate mortar and pestle for approximately 40 min to achieve a uniform mixture; then 0.15 mL paraffin oil was added and the paste stirred with a glass rod. The homogenized mixture was transferred to 3 mm inner diameter glass tubes, and the mixture was

pressed into a length of 0.8 cm by the use of a copper stick. The tube surface was wiped with weighing paper, and the electrical contact was established with a copper stick through the back of the electrode.

Supporting information

A scheme of the ligand skeleton, additional crystal structure plots, IR spectra, TG curves, emission spectra of **1–3**, a plot of the cathodic/anodic peak currents of **1**-CPE as well as a compilation of bond lengths and angles in the crystal structures of **1–3** are given as Supporting Information available online (DOI: 10.5560/ZNB.2013-3007).

Acknowledgement

Financial support of this research by the National Natural Science Foundation of China (no. 21171025 and 21101015), New Century Excellent Talents in University (NCET-09-0853), the Natural Science Foundation (201102003), the Doctoral Initiation Project of Liaoning Province (20111147), and the Program of Innovative Research Team in University of Liaoning Province (LT2012020) is gratefully acknowledged.

- [1] C. Ritchie, A. Ferguson, H. Nojiri, H. Miras, Y. F. Song, D. L. Long, E. Burkholder, M. Murrie, P. Kögerler, E. K. Brechin, L. Cronin, *Angew. Chem. Int. Ed.* **2008**, *47*, 5609–5612.
- [2] B. S. Bassil, M. Ibrahim, R. Oweini, M. Asano, Z. X. Wang, J. Tol, N. S. Dalal, K. Y. Choi, R. N. Biboum, B. Keita, L. Nadjo, U. Kortz, *Angew. Chem. Int. Ed.* **2011**, *50*, 5961–5964.
- [3] T. Hirano, K. Uehara, K. Kamata, N. Mizuno, *J. Am. Chem. Soc.* **2012**, *134*, 6425–6433.
- [4] F. J. Ma, S. X. Liu, C. Y. Sun, D. D. Liang, G. J. Ren, F. Wei, Y. G. Chen, Z. M. Su, *J. Am. Chem. Soc.* **2011**, *133*, 4178–4181.
- [5] H. Y. Liu, H. Wu, J. Yang, Y. Y. Liu, J. F. Ma, H. Y. Bai, *Cryst. Growth Des.* **2011**, *11*, 1786–1797.
- [6] X. J. Kong, Y. P. Ren, P. Q. Zheng, Y. X. Long, L. S. Long, *Inorg. Chem.* **2006**, *45*, 10702–10711.
- [7] X. L. Hao, M. F. Luo, W. Yao, Y. G. Li, Y. H. Wang, E. B. Wang, *Dalton Trans.* **2011**, *40*, 5971–5976.
- [8] H. Y. An, Y. G. Li, E. B. Wang, D. R. Xiao, C. Y. Sun, L. Xu, *Inorg. Chem.* **2005**, *44*, 6062–6070.
- [9] J. Q. Sha, J. Peng, Y. Q. Lan, Z. M. Su, H. J. Pang, A. X. Tian, P. P. Zhang, M. Zhu, *Inorg. Chem.* **2008**, *47*, 5145–5153.
- [10] H. Y. An, Y. G. Li, D. R. Xiao, E. B. Wang, C. Y. Sun, *Cryst. Growth Des.* **2006**, *6*, 1107–1112.
- [11] L. M. Dai, W. S. You, E. B. Wang, S. X. Wu, Z. M. Su, Q. H. Du, Y. Zhao, Y. Fang, *Cryst. Growth Des.* **2009**, *9*, 2110–2116.
- [12] X. L. Wang, H. L. Hu, G. C. Liu, H. Y. Lin, A. X. Tian, *Chem. Commun.* **2010**, *46*, 6485–6487.
- [13] X. L. Wang, H. L. Hu, A. X. Tian, H. Y. Lin, J. Li, *Inorg. Chem.* **2010**, *49*, 10299–10306.
- [14] X. L. Wang, H. L. Hu, A. X. Tian, *Cryst. Growth Des.* **2010**, *10*, 4786–4794.
- [15] X. L. Wang, Q. Gao, A. X. Tian, G. C. Liu, *Cryst. Growth Des.* **2012**, *12*, 2346–2354.
- [16] X. L. Wang, Y. F. Wang, G. C. Liu, A. X. Tian, *Dalton Trans.* **2011**, *40*, 9299–9305.
- [17] X. Wang, J. Peng, M. G. Liu, D. D. Wang, C. L. Meng, Y. Li, Z. Y. Shi, *CrystEngComm* **2012**, *14*, 3220–3226.
- [18] J. Q. Sha, L. Y. Liang, J. W. Sun, A. X. Tian, P. F. Yan, G. M. Li, C. Wang, *Cryst. Growth Des.* **2012**, *12*, 894–901.
- [19] I. D. Brown, D. Altermatt, *Acta Crystallogr. B* **1985**, *41*, 244–247.
- [20] A. X. Tian, J. Ying, J. Peng, J. Q. Sha, H. J. Pang, P. P. Zhang, Y. Chen, M. Zhu, Z. M. Su, *Cryst. Growth Des.* **2008**, *8*, 3717–3724.
- [21] X. J. Kong, Y. P. Ren, P. Q. Zheng, Y. X. Long, L. S. Long, R. B. Huang, L. S. Zheng, *Inorg. Chem.* **2006**, *45*, 10702–10711.

- [22] Y. G. Li, L. M. Dai, Y. H. Wang, X. L. Wang, E. B. Wang, Z. M. Su, L. Xu, *Chem. Commun.* **2007**, 25, 2593–2595.
- [23] X. L. Wang, C. Xu, H. Y. Lin, G. C. Liu, Y. Song, Q. Gao, A. X. Tian, *CrystEngComm* **2012**, 14, 5836–5844.
- [24] Y. Bai, G. Q. Zhang, D. B. Dang, P. Y. Ma, H. Gao, J. Y. Niu, *CrystEngComm* **2011**, 13, 4181–4187.
- [25] B. K. Tripuramallu, R. Kishore, S. K. Das, *Inorg. Chim. Acta* **2011**, 368, 132–140.
- [26] X. L. Wang, J. Li, A. X. Tian, D. Zhao, G. C. Liu, H. Y. Lin, *Cryst. Growth Des.* **2011**, 11, 3456–3462.
- [27] X. L. Wang, Y. F. Bi, B. K. Chen, H. Y. Lin, G. C. Liu, *Inorg. Chem.* **2008**, 47, 2442–2448.
- [28] Y. Hu, F. Luo, F. F. Dong, *Chem. Commun.* **2011**, 47, 761–763.
- [29] G. M. Sheldrick, *Acta Crystallogr.* **2008**, A64, 112–122.
- [30] Q. G. Zhai, X. Y. Wu, S. M. Chen, Z. G. Zhao, C. Z. Lu, *Inorg. Chem.* **2007**, 46, 5046–5058.
- [31] Y. N. Chi, F. Y. Cui, A. R. Jia, X. Y. Ma, C. W. Hu, *CrystEngComm* **2012**, 14, 3183–3188.
- [32] J. Zhao, J. S. Wang, J. W. Zhao, P. T. Ma, J. P. Wang, J. Y. Niu, *Dalton Trans.* **2012**, 41, 5832–5837.
- [33] X. L. Wang, Z. H. Kang, E. B. Wang, C. W. Hu, *Mater. Lett.* **2002**, 56, 393–396.